This article has been accepted for publication in IEEE Transactions on Neural Systems and Rehabilitation Engineering. This is the author's version which has not been fully edited and content may change prior to final publication. Citation information: DOI 10.1109/TNSRE.2023.3332114

Rehabilitation Modulates High-Order Interactions among Large-Scale Brain Networks in Subacute Stroke

I. Pirovano, Y. Antonacci, A. Mastropietro*, C. Barà, L. Sparacino, *Student Member, IEEE,* E. Guanziroli, F. Molteni, M. Tettamanti, L. Faes, *Senior Member, IEEE*, G. Rizzo

***Abstract*—The recovery of motor functions after stroke is fostered by the functional integration of large-scale brain networks, including the motor network (MN) and high-order cognitive controls networks, such as the default mode (DMN) and executive control (ECN) networks. In this paper, electroencephalography signals are used to investigate interactions among these three resting state networks (RSNs) in subacute stroke patients after motor rehabilitation. A novel metric, the O-information rate (OIR), is used to quantify the balance between redundancy and synergy in the complex high-order interactions among RSNs, as well as its causal decomposition to identify the direction of information flow. The paper also employs conditional spectral Granger causality to assess pairwise directed functional connectivity between RSNs. After rehabilitation, a synergy increase among these RSNs is found, especially driven by MN. From the pairwise description, a reduced directed functional connectivity towards MN is enhanced after treatment. Besides, inter-network connectivity changes are associated with motor recovery, for which the mediation role of ECN seems to play a relevant role, both from pairwise and high-order interactions perspective.**

***Index Terms*—EEG, functional connectivity, Granger Causality, high-order interactions, redundancy, rehabilitation, resting-state networks, synergy, stroke.**

I. INTRODUCTION

The identification of large-scale functional brain networks and the investigation of the interactions among different cerebral areas within and across these networks are of increasing interest to characterize neurophysiological mechanisms both in physiological and pathological conditions. In the field of computational neuroscience, a common strategy adopted to characterize complex interactions among a large number of brain regions is to build network models where pairwise relations are considered, and where metrics derived from graph theory [1] are calculated to describe the collective behavior of the networks. The pairwise approach is very useful to detect and reconstruct causal networks in physiology [2] and neuroscience [3]. A major limitation of this approach, however, is that pairwise measures cannot detect high-order interactions (HOIs), i.e., interactions involving three or more network nodes [4]. There is increasing evidence that interactions within the brain involve more than two areas simultaneously, and that a collective emerging behavior is exhibited at different levels of integration [5], [6]. Therefore, pairwise strategies appear limited for the description of a complex system such as the brain, and high-order functional connectivity approaches should be instead adopted [7]. Different measures of HOIs have been defined in the field of information theory for multiple time series. Interaction information (II) [8] and partial information decomposition (PID) [9] are the most widely employed approaches to account for interactions among three random variables. Typically, these approaches describe the redundant or synergistic behavior limited to a group of three processes [10]. Broadly speaking, synergy arises when the interactions found observing the global system are stronger than those observed in parts of it, while redundancy refers to interactions of sub-groups of variables which explain fully the overall shared information [11]. The II approach provides a compact metric which describes the balance between redundancy and synergy in a network of three random variables: positive values of II indicate a predominance of redundancy, while negative values suggest a prevalence of synergy in the observed system. In 2019, Rosas *et al.* [10] proposed the O-information (OI) metric as an extension of II to more than three interacting variables. More recently, Faes *et al.* [11] introduced the O-Information Rate (OIR), that is an extension to spectral causal decomposition as a further generalization of II to also account for random processes. This new metric allows to obtain both time-domain and spectral measures of high-order functional connectivity in a system of multivariate processes.

HOIs analysis has already been applied, in the context of both II and PID, to a few neuroimaging studies employing functional

The work was funded in part by Fondazione Cariplo and Regione Lombardia, Progetto "Active[3] - Everyone, Everywhere, Everyday", Ref. (2021-0612) and in part by SiciliAn MicronanOTecH Research And Innovation CEnter "SAMOTHRACE" (MUR, PNRR-M4C2, ECS_00000022), spoke 3 - Università degli Studi di Palermo "S2-COMMs - Micro and Nanotechnologies for Smart & Sustainable Communities".

I. Pirovano, A. Mastropietro and G. Rizzo are with the Institute of Biomedical Technology, National Research Council, Segrate, Milan, Italy (*corresponding author e-mail: alfonso.mastropietro@itb.cnr.it).

Y. Antonacci, C. Barà, L. Sparacino and L. Faes are with the Department of Engineering, University of Palermo, Palermo, Italy.

E. Guanziroli and F. Molteni are with Villa Beretta Rehabilitation Center, Ospedale Valduce, Costa Masnaga, Lecco, Italy.

M. Tettamanti is with the Department of Psychology University of Milano-Bicocca, Milan, Italy.

This work is licensed under a Creative Commons Attribution-NonCommercial-NoDerivatives 4.0 License. For more information, see https://creativecommons.org/licenses/by-nc-nd/4.0/

This article has been accepted for publication in IEEE Transactions on Neural Systems and Rehabilitation Engineering. This is the author's version which has not been fully edited and content may change prior to final publication. Citation information: DOI 10.1109/TNSRE.2023.3332114

magnetic resonance imaging (fMRI) and electroencephalography (EEG) [4], [12]–[15]. Most of these studies characterized HOIs among different resting state networks (RSNs) in healthy subjects. However, these metrics could also provide interesting information in the investigation of brain conditions known to cause disruption in large-scale networks, as in the case of healthy brain aging [13] and dementia or Alzheimer's disease [4]. Besides neurodegenerative diseases, other pathologies are known to cause brain networks disruptions. For example, the effects of cerebrovascular stroke on brain functional connectivity are widely investigated, due to the high incidence of stroke in the worldwide population and to the impact of resultant impairments on the quality of life of stroke survivors [16]. However, high-order functional connectivity approaches have not been yet applied to investigate stroke effects and the associated neuro-plasticity changes involved in recovery. To the best of our knowledge, findings reported in the literature about cerebrovascular stroke were exclusively based on metrics of pairwise interaction between signals, either from fMRI or EEG techniques, in brain regions belonging to different resting-state sub-networks [17]. In particular, great attention has been given to the evaluation of recovery-related changes within the motor network (MN) [18], since more than a half of stroke survivors experience motor deficits [19]. However, the brain is a complex system, and it has been demonstrated that disruption of connections between large-scale RSNs may as well contribute to post-stroke impairments [20]. A few studies have investigated both within and between large-scale RSNs connectivity patterns in stroke populations [20]–[22]. In these works, altered functional connectivity has been found among different brain areas including not only sensory and sensorimotor cortices, but also high-order cognitive control networks such as the default mode network (DMN), the executive control network (ECN), and the dorsal attention network [21], [23]. The MN is primarily responsible for the execution of motor tasks and to this aim it integrates sensorimotor information [24]. The DMN mediates interoceptive monitoring and self-referential processes, and is involved in the integration of perceptual information for higher-order cognitive processes [25]. The ECN is involved in the control and execution of externally directed activities [26], and exerts control over posterior sensorimotor representations to drive information selection and maintenance for behavioral responses [27]. The disruption of interactions among these three RSNs appears to be related to motor and cognitive impairments in stroke, and these interactions may play a relevant role in the cerebral reorganization associated with functional recovery after stroke [28]. In fact, correlations between motor functionality recovery and the strengths of connections between pairs of areas belonging to the motor cortex and higher-order control networks have already been observed in fMRI studies on subacute stroke patients following a Brain-Computer Interface rehabilitation training [29]. Moreover, it has been observed that some cognitive control regions show higher activity in the acute phase of stroke and in the process of motor recovery, as compared to controls, whereas increased functional connectivity in the ipsilesional areas of the ECN negatively correlate with upper limb motor recovery scales [22], [28]. As for the role of the DMN, some evidence of inter-network alterations of the DMN interaction with sensory-motor areas have been recently found in stroke patients [22]. Even though the role of the DMN in post-stroke motor deficit needs further investigation, fronto-parietal regions have been found to play a role in the recovery of motor function in stroke patients by providing compensatory neural pathways when traditional connections are compromised [30]. All these results have been obtained evaluating pairwise functional connectivity, mostly based on fMRI data. However, none of the above-mentioned studies have considered jointly the concurrent interactions between these three networks, and a longitudinal study on the effects of rehabilitation on HOIs is missing.

In the present work, we propose to investigate changes ensuing from post-stroke rehabilitation in the interactions among the three above-mentioned RSNs, by applying high-order metrics and thus going beyond the traditional pairwise analysis. In detail, we analyzed changes in cortical connectivity estimated from resting state EEG signals in a cohort of patients in the subacute post-stroke stage who followed a period of physical rehabilitation. Considering the high temporal resolution of EEG signals, we exploited the OIR metric to perform a causal and spectral high-order connectivity analysis of the temporal dynamics among large-scale brain networks.

II. Materials and Methods

A. Participants

Eighteen post-stroke patients participated in this study, which was approved by the local Ethics Committee "Comitato Etico Provinciale dell'Insubria" and conducted in compliance with the Declaration of Helsinki. Participants (7 females and 11 males, aged 67 ± 10 (mean ± std) years) were all enrolled in the subacute stage after a single unilateral ischemic stroke and met the inclusion criteria of occurrence of the acute event less than 30 days after the first evaluation. All subjects were right-handed, had no other reported concomitant orthopedic or rheumatologic diseases, and had no global or comprehension aphasia. Each patient followed a physical rehabilitation treatment for both upper and lower limbs, tailored according to the individual residual motor capacity. More details about the dataset can be found in Ref. [31].

B. Clinical performance assessment

Subjects were evaluated by clinicians both from a clinical and an electrophysiological point of view at two time-points: at the admission to the rehabilitation center (T0, on average after 12 ± 5 days from the stroke event) and at the end of the treatment (T1, on average after 55 ± 11 days from the stroke event). The upper limb performance was evaluated with the upper extremities Fugl-Meyer Assessment (FMA), which includes a motor scale with scores ranging from 0 (hemiplegia) to 66 (normal motor performance) [32]. Likewise, the level of walking ability was assessed by the Functional Ambulation Category (FAC), a gait assessment scale that distinguishes

This work is licensed under a Creative Commons Attribution-NonCommercial-NoDerivatives 4.0 License. For more information, see https://creativecommons.org/licenses/by-nc-nd/4.0/

This article has been accepted for publication in IEEE Transactions on Neural Systems and Rehabilitation Engineering. This is the author's version which has not been fully edited and content may change prior to final publication. Citation information: DOI 10.1109/TNSRE.2023.3332114

TABLE I
REGIONS OF INTEREST

RSN[a]	Region	Coordinates in mm (X, Y, Z)	Number of voxels
DMN	PCC/precuneus	0, -52, 27	14
	Medial Prefrontal	-1, 54, 27	13
	L Lateral Parietal	-46, -66, 30	12
	R Lateral Parietal	49, -63, 33	8
	L Middle Temporal	-61, -24, -9	15
	R Middle Temporal	58, -24, -9	12
ECN	Dorsal Medial PFC	0, 24, 46	15
	L Anterior PFC	-44, 45, 0	7
	R Anterior PFC	44, 45, 0	6
	L Inferior parietal	-50, -51, 45	13
	R Inferior parietal	50, -51, 45	16
MN	L M1	-33, -20, 52	12
	R M1	-36, -18, 52	13
	L PreMotor	-34, -1, 56	13
	R PreMotor	35, 0, 55	13
	SMA	0, -4, 65	10

Cerebral areas grouped by large-scale networks. Centroids coordinates (X, Y, Z) are reported in the MNI coordinate system.
[a]RSN = Resting-State Network, DMN = Default Mode Network, ECN = Executive Controls Network, MN = Motor Network, PCC = Posterior Cingulate Cortex, PFC = pre-frontal cortex, M1 = primary motor cortex, SMA = Supplementary Motor Area, L = left, R = right.

between 6 levels of walking ability (0, not able to walk; 5, independent walk) based on the amount of physical support required [33]. The variations $FMA^{T1\text{-}T0} = FMA^{T1} - FMA^{T0}$ and $FAC^{T1\text{-}T0} = FAC^{T1} - FAC^{T0}$ were considered as primary clinical outcomes of subject's motor recovery.

C. EEG acquisition, pre-processing and source reconstruction

At both T0 and T1, 5 minutes of eye-closed resting state EEG recordings were collected with a Neuroscan system (Compumedics Neuroscan, Compumedics, NC, USA). 64 Ag/AgCl electrodes were placed on the scalp according to the International 10/20 standard system with the reference electrode placed between Fz and Cz positions and the ground electrode positioned anterior to Fz. Continuous data were acquired at a sampling rate of 1000 Hz.

EEG signals were pre-processed offline in Matlab (The Mathworks, Inc.) using the open source EEGLab signal processing Toolbox [34]. Data were down-sampled at 128 Hz and band-pass filtered between 0.5 Hz and 45 Hz to remove slow drifts and high-frequency components. Flat (zero amplitude for more than 5 s) and "bad" (noisy for more than 90% of the acquisition) channels were removed and the Artifacts Subspace Reconstruction (ASR) algorithm [35] was applied to all retained channels with a cut-off parameter $k = 20$. Independent Component Analysis (ICA) was then applied to the ASR-cleaned EEG exploiting the RUNICA Infomax algorithm [36], and the ICLabel automated classifier [37] was employed to guide the manual selection of non-brain artifactual components, e.g., eye, heart, muscle, line noise. The originally removed channels were reconstructed by the interpolation of the neighbor signals and the cleaned EEG data were re-referenced to a common average value. For all the acquisitions, the first 30 s were discarded to account for a period of settling before reaching the proper resting state condition and the subsequent 1 min was used for brain sources estimation. We employed the exact low resolution brain electromagnetic tomography (eLORETA) approach, which allows the exact localization of the brain current source densities distribution implementing a discrete, linear, weighted minimum norm inverse solution [38]. Activity of brain sources was reconstructed only in the cortical grey matter (6239 isotropic voxels with 5 mm spatial resolution) in the MNI152 space.

D. Regions of interest and time series extraction

For the inter-network connectivity analysis, 16 Regions of Interest (ROIs) have been chosen according to the previous literature on RSNs identification [39]–[41]. In table I, centroid coordinates in the MNI152 space and number of voxels of 6 ROIs within DMN, 5 ROIs belonging to ECN, and 5 ROIs within MN are reported Considering that EEG measurement sensibility is largely confined to superficial cortical areas, we excluded from the analysis deeper cerebral structures such as cerebellum and basal nuclei, as proposed in [41]. All voxels within 8 mm of radius from a seed were considered as belonging to the specific ROI, with the constraint of non-overlapping regions [41]. In case of overlap, the voxels were assigned to the closest centroid regions. Sixteen time series of 7680 samples (1 min) each were thus obtained, by averaging the magnitude of sources activity among all voxels belonging to each ROI. For further analysis, the ROI signals were epoched in shorter windows of 10 s, hence obtaining 6 windows of 1280 samples for each acquisition.

E. Connectivity analysis

We performed an inter-network resting state connectivity analysis, considering the three subsets of ROIs, grouped as reported in Table I, as vector targets constituting a three-node RSN. Both pairwise and high-order analysis were conducted in a linear parametric framework based on linear Multivariate Autoregressive (MVAR) modeling of multiple time series, under the assumption of wide-sense stationarity and of jointly Gaussian stochastic processes. The analysis follows the OIR framework introduced in Ref.[11].

1) MVAR models

Let us consider a set of Q stochastic processes, $\boldsymbol{Y} = [Y_1, \ldots, Y_Q]^T$ grouped in M blocks $\boldsymbol{X} = [X_1, \ldots, X_M]^T$ (Q=16, M=3 in this work). In the linear signal processing frame, the processes can be described by the MVAR model

$$\boldsymbol{Y}(n) = \sum_{k=1}^{p} \boldsymbol{A}(k) Y(n-k) + \boldsymbol{U}(n), \qquad (1)$$

where p is the model order, $\boldsymbol{A}(k)$ is a Q×Q matrix of coefficients $A_{ij}(k)$ describing the dependence of $Y_i(n)$ on $Y_j(n-k)$ (i,j = 1,…, Q), and $\boldsymbol{U}(n)$ is a Q×1 vector of uncorrelated white noises with Q×Q covariance matrix $\boldsymbol{\Sigma}_U = \mathbb{E}[\boldsymbol{U}(n)\boldsymbol{U}(n)^T]$. Note that, while the MVAR model (1) gives an explicit representation of the overall multivariate process $\boldsymbol{Y}$ collecting Q=16 ROIs, information about the interactions between the M=3 subsets of

This work is licensed under a Creative Commons Attribution-NonCommercial-NoDerivatives 4.0 License. For more information, see https://creativecommons.org/licenses/by-nc-nd/4.0/

This article has been accepted for publication in IEEE Transactions on Neural Systems and Rehabilitation Engineering. This is the author's version which has not been fully edited and content may change prior to final publication. Citation information: DOI 10.1109/TNSRE.2023.3332114

RSNs can be extracted considering the blocks grouped in $\boldsymbol{X}$.

The linear parametric representation of the observed processes can be translated in the frequency domain taking the Fourier Transform (FT) of (1), which yields

$$\boldsymbol{Y}(\omega) = \boldsymbol{A}(\omega)\boldsymbol{Y}(\omega) + \boldsymbol{U}(\omega), \quad (2)$$

where $\boldsymbol{Y}(\omega)$ and $\boldsymbol{U}(\omega)$ are the FTs of $\boldsymbol{Y}(n)$ and $\boldsymbol{U}(n)$, $\omega \in [-\pi, \pi]$ is the normalized angular frequency, and $\boldsymbol{A}(\omega) = \sum_{k=1}^{p} A(k)e^{-j\omega}$ provides the spectral representation of the coefficients, from which the model transfer function can be defined as: $\boldsymbol{H}(\omega) = [\boldsymbol{I} - \boldsymbol{A}(\omega)]^{-1}$ [42]. The $Q \times Q$ power spectral density (PSD) matrix is then computed using spectral factorization as:

$$\boldsymbol{S}(\omega) = \boldsymbol{H}(\omega)\boldsymbol{\Sigma}_U\boldsymbol{H}^*(\omega), \quad (3)$$

where $*$ indicates the Hermitian transpose. From this vectorial AR representation of multiple time series and from the derived PSD matrix we can calculate both pairwise and high-order metrics of directed and undirected functional connectivity among the subsets of signals forming each analyzed RSN.

2) Pairwise interactions

To assess the directed functional connectivity between the three chosen RSNs, we exploited the concept of Granger causality (GC) [43]. To compute it, the reduced bivariate AR model describing the interactions between X_i and X_j is obtained in the framework of state-space models directly from the parameters of the overall VAR model (1) (see Ref. [11] for details). Then, since we are interested in the study of connectivity at specific rhythmic components of the neural signals, such model is converted in the frequency domain to obtain its transfer function $\boldsymbol{H}(\omega)$, which is exploited to compute the logarithmic spectral measure of GC (sGC) from X_j to X_i as [44]:

$$f_{j\to i}(\omega) = \ln \frac{|\boldsymbol{S}_i(\omega)|}{\left|\boldsymbol{H}_{ii}(\omega)\boldsymbol{\Sigma}_{W_i}(\omega)\boldsymbol{H}_{ii}^*(\omega)\right|}, \quad (4)$$

where $\boldsymbol{S}_i(\omega)$ is the PSD of X_i, $\boldsymbol{H}_{ii}(\omega)$ is the transfer function of the reduced bivariate AR model at specific frequency ω, and $\boldsymbol{\Sigma}_{W_i}$ the covariance matrix of the error resulting from the prediction of X_i in the reduced model. The reduced bivariate AR model can be exploited also to compute the spectral GC from X_j to X_i, $f_{j\to i}(\omega)$, as well as the Geweke measure of total (undirected) dependence between the two processes, which takes the form

$$f_{i,j}(\omega) = \ln \frac{|\boldsymbol{S}_{ii}(\omega)||\boldsymbol{S}_{jj}(\omega)|}{|\boldsymbol{S}(\omega)|}. \quad (5)$$

This total dependence measure is related to the two GC measures by the spectral decomposition [44], [45]:

$$f_{i,j}(\omega) = f_{i\to j}(\omega) + f_{j\to i}(\omega) + f_{i\cdot j}(\omega), \quad (6)$$

where $f_{i\cdot j}(\omega)$ quantifies the instantaneous interactions between X_i and X_j expanded in the frequency domain [11].

Moreover, in a multivariate framework as the one here considered, it is important to compute also the conditional measure of spectral GC (csGC), $f_{j\to i|\boldsymbol{Z}}(\omega)$, as defined in [46], whereby the causal interaction from X_j to X_i is conditioned to all other processes collected in the vector $\boldsymbol{Z} = \boldsymbol{Y}\backslash\{X_i, X_j\}$. This measure allows to rule out indirect causality links possibly arising along the pathway from X_j to X_i due to the other processes contained in $\boldsymbol{Z}$. It can be computed combining the full VAR model (1) with a reduced model in which X_j is removed; again, calculations can be performed efficiently in the framework of state space models [11]. In this work, considering only the direct inter-network links estimated by csGC, we provide an indication of the net flow of information exchanged by two subsets of ROIs, i.e., two RSNs, calculating a Net Flow Index (NFI) for the i-th node as the difference between the csGC computed along the two directions of interaction:

$$NFI_{w_i}(\omega) = f_{i\to j|\boldsymbol{Z}}(\omega) - f_{j\to i|\boldsymbol{Z}}(\omega)\,. \quad (7)$$

3) HOIs

In this works, the analysis of HOIs is performed through the spectral O-information rate (OIR), following the framework proposed in [11], which we briefly recall here particularized to the case implemented in this work which considers three interacting vector processes. Specifically, at each frequency, the spectral OIR among the processes $\{X_1, X_2, X_3\}$ is defined as:

$$\nu_{X_1;X_2;X_3}(\omega) = f_{X_i;X_j}(\omega) + f_{X_i;X_k}(\omega) - f_{X_i;X_j,X_k}(\omega) \quad (8)$$

where the three terms in the r.h.s. of (8) correspond to the spectral function of total coupling (5) computed between X_i and X_j,X_k either taken separately or together ($i, j, k \epsilon \{1,2,3\}$).

The OIR is a symmetric measure, hence it does not provide information on the direction of the influence of one group of processes over another. However, the spectral OIR gradient can be decomposed as the sum of three terms:

$$\nu_{X_1;X_2;X_3}(\omega) = \delta_{X_i\to X_j,X_k}(\omega) + \delta_{X_j,X_k\to X_i}(\omega) + \delta_{X_i\cdot X_j,X_k}(\omega), \quad (9)$$

which account for the directed information transfer from X_i to X_j,X_k and vice-versa, and for the instantaneous interactions shared by the processes. The three terms are obtained expanding the spectral functions in (8) according to (6) [11]. Both the OIR and the terms of its decomposition provide an informational character, which is redundant when the term is positive, and synergistic when the term is negative. Importantly, the spectral OIR is closely related to the time-domain measures of total coupling resulting from the full-frequency integration of the three spectral coupling functions in (8), in a way such that a time-domain OIR measure, $\Omega_{X_1;X_2;X_3}$, can be obtained integrating $\nu_{X_1;X_2;X_3}(\omega)$ over all frequencies ($\omega \in [-\pi, \pi]$). An analogous integration can be applied to (9) to obtain time-domain measures of directed and instantaneous information transfer. Again, all these time-domain measures reflect the redundant (when positive) or synergistic (when negative) character of the information shared and transferred among the processes [11].

This work is licensed under a Creative Commons Attribution-NonCommercial-NoDerivatives 4.0 License. For more information, see https://creativecommons.org/licenses/by-nc-nd/4.0/

This article has been accepted for publication in IEEE Transactions on Neural Systems and Rehabilitation Engineering. This is the author's version which has not been fully edited and content may change prior to final publication. Citation information: DOI 10.1109/TNSRE.2023.3332114

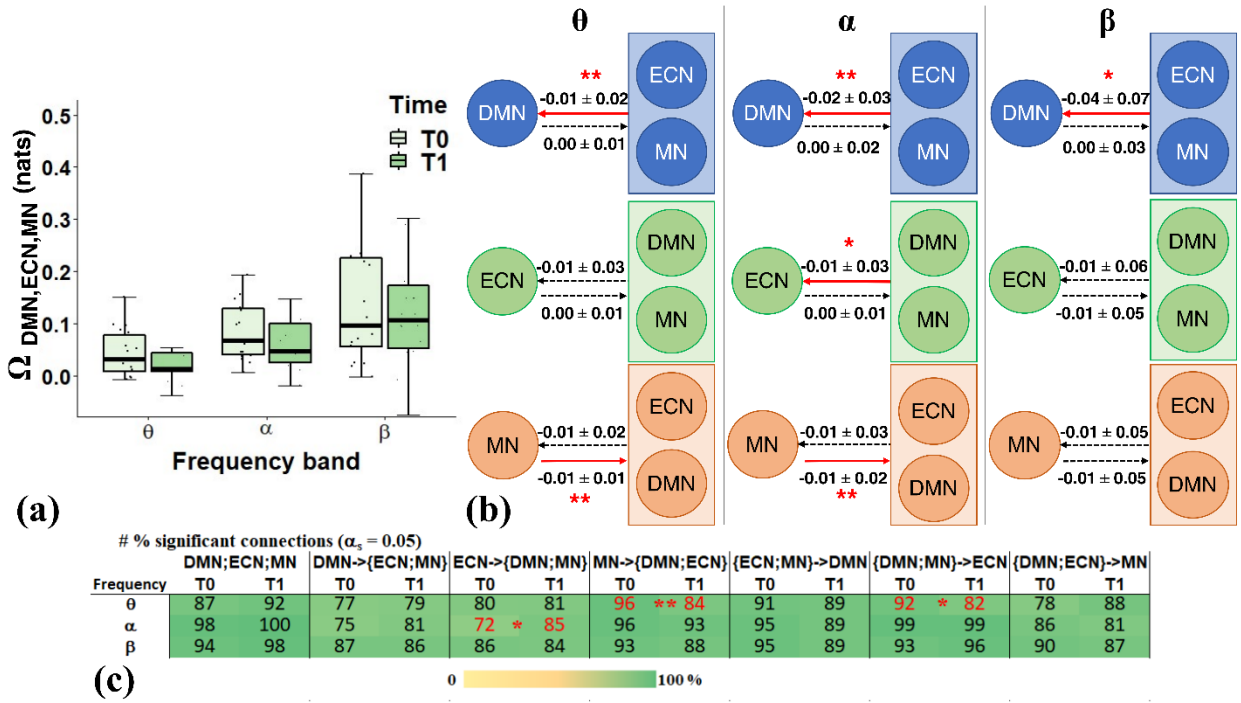

Fig. 1. (a) Total OIR distribution $\Omega_{DMN,ECN,MN}$ of the population integrated for each frequency band. Boxplot lengths represent the interquartile range (IQR), horizontal line corresponds to the median value, the external whiskers include data within ±1.5×IQR. (b) Causal decomposition of the spectral OIR gradient. Population average differences $\Omega^{T1\text{-}T0}$ are reported as mean ± std when DMN (first row), ECN (second row), and MN (third row) act as single target with respect to the rest of the system for θ, α, and β frequency bands (in columns). Red arrows indicate significant T1 – T0 differences. *, p-value < 0.05, **, p-value < 0.01. When average differences values of 0.00 are indicated, this corresponds to an average $\Omega^{T1\text{-}T0} < 10^{-2}$. (c) Modified IAAFT surrogates' population analysis for HOIs measure. For each frequency, percentages of statistically significant interactions in the whole population are reported at both T0 and T1. Asterisks indicate a statistically T1 – T0 difference according to McNemar test, *, p-value < 0.05, **, p-value < 0.01.

F. Data Analysis and statistical analysis

In this work, all measures of interactions were computed identifying the MVAR model (1) through the least square method [11]. The Akaike information criterion (AIC) was used to select the optimum order p for each epoch of the acquired resting state signals. Conditional spectral GC (csCG), and spectral OIR $\nu_{X_1;X_2;X_3}(\omega)$ with the causal decomposition terms of its gradient, $\delta_{X_i \to X_j,X_k}(\omega)$ and $\delta_{X_j,X_k \to X_i}(\omega)$, were calculated among the three RSNs separately for each of the six signals' epochs, at T0 and T1. Then, measures were integrated over the range of the three frequencies of interest, i.e., theta (θ), alpha (α), and beta (β), thus obtaining the equivalent metrics in time-domain at the specific oscillation, $\Omega_{X_1;X_2;X_3}(\omega)$. Delta and gamma bands were excluded from this analysis since they may be affected by noise and spurious signals. To account for interindividual variability, frequency bands ranges were defined according to the Individual Alpha Frequency (IAF) criteria [47] as follows: θ = [IAF-6 Hz ÷ IAF-2.5 Hz], α = [IAF-2 Hz ÷ IAF+2 Hz], and β = [IAF+2.5 Hz ÷ IAF+20 Hz].

The six epoch values were finally averaged to obtain one value per acquisition per subject. Considering the small sample size, we employed non-parametric statistical tests to assess the rehabilitation effect in terms of inter-networks connectivity changes. To control for spurious estimation, we tested the statistical significance of the estimated connections with the surrogates' data approach [48]. For HOIs, we implemented a modified Iterative Adjusted Amplitude Fourier Transform (IAAFT) surrogate approach, which exploits the phase randomization procedure to satisfy the null hypothesis of balanced high-order interactions (absence of net redundancy or net synergy leading to null OIR) in a given frequency band, preserving the pairwise correlations within each RSN. Specifically, we applied phase randomization by summing the same random number to the Fourier phases of all signals belonging to a randomly chosen RSN, leaving untouched the signals of the two other RSNs. This preserved the auto- and cross-correlations within the block subjected to phase randomization, as well as the auto- and cross-correlations within and between the two other blocks. This procedure was iteratively applied 100, choosing randomly the block to be subjected to phase randomization, and thus creating a surrogate distribution of data.

As for pairwise interactions, i.e., csGC values, the causal Fourier Transform (CFT) method [49] was used to generate 100 surrogates time series, with the null hypothesis of absence of direct causal coupling in a given frequency band, for each link between two RSNs. With this approach, all individual correlations, as well as the directed correlations along other directions different than the observed one, were preserved.

To test for statistical significance with a confidence level α_s = 0.05, we compared the OIR values estimated for the original data with the 5th percentile, when OIR < 0, and 95th percentile, when OIR > 0, of their surrogate distribution. csGC values obtained for the original distribution were compared with the 95th percentile of surrogate distribution. This procedure was repeated for each frequency, for data both pre- and post-rehabilitation. Connections above the threshold were put to 1

This work is licensed under a Creative Commons Attribution-NonCommercial-NoDerivatives 4.0 License. For more information, see https://creativecommons.org/licenses/by-nc-nd/4.0/

This article has been accepted for publication in IEEE Transactions on Neural Systems and Rehabilitation Engineering. This is the author's version which has not been fully edited and content may change prior to final publication. Citation information: DOI 10.1109/TNSRE.2023.3332114

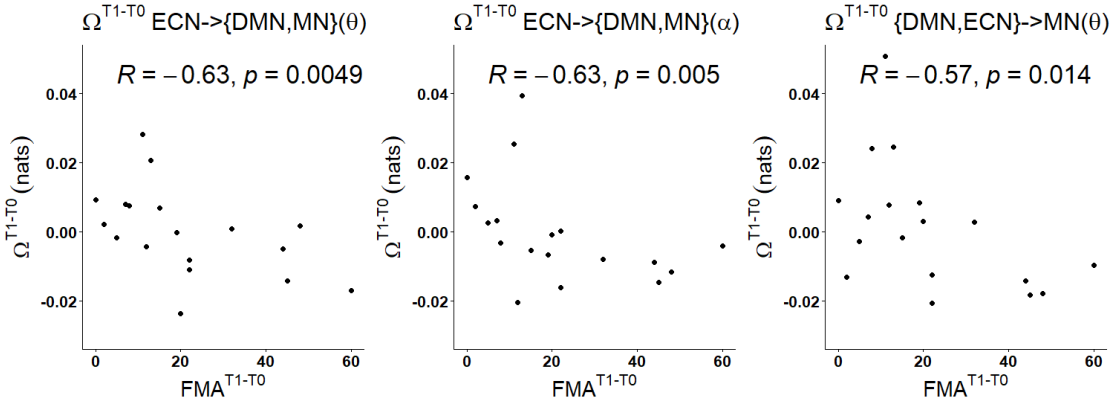

Fig. 2 Significant Spearman's correlations between OIR variations T1-T0 and FMA^{T1-T0}. R, correlation coefficient, p, p-value.

and connections below were put to 0. Thus, we obtained binarized spectral connectivity matrices of significant HOIs and pairwise directed connections for each subject pre and post-rehabilitation.

Then, we calculated the percentage of subjects for whom each connection turned out significant. We statistically compared the variation of population number of significant connections (Δ#) from T0 to T1 with the non-parametric McNemar Test for binomial data. Besides, T0 and T1values of all connectivity metrics, OIR and pairwise csGC were compared by a non-parametric one-tailed Wilcoxon's test for paired samples. To further investigate the correlations of inter-network connectivity changes with the functional outcomes, non-parametric Spearman's correlations between the variation of both pairwise ($csGC^{T1-T0}$) and high-order (Ω^{T1-T0}) connectivity metrics with FMA^{T1-T0} and FAC^{T1-T0} scores were computed. The statistical significance level was set at 0.05 for all tests. Because of the small sample size, in this work we did not correct the p-values from our statistical analysis for family-wise error rate. This could increase the chance of type I error, but we aimed to avoid missing any potential significance in our exploratory analysis. Therefore, we highlighted the stronger significance values ($p < 0.01$) in the results section.

III. Results

Hereafter, we firstly report the results obtained for the high-order analysis, followed by the pairwise description on the inter-network directed functional connectivity. For each measure, correlation analysis results with motor outcomes are also reported. In Fig. 1, we report the population distributions of global OIR $\Omega_{DMN,ECN,MN}$ in the three frequency bands (a), its causal decomposition (b) and the percentages of statistically significant interactions estimated for the population according to surrogate data analysis (c). As can be seen in Fig.1(c), more than 70% of estimated HOIs resulted to be statistically significant, thus detecting the presence of unbalanced high-order interactions, with prevalence of redundancy over synergy. Moreover, we found a significant variation of the statistical representation of a few causal interactions. We observe an increased significant representation of ECN when it acts as the single driver towards the system {DMN,MN} in α, whereas a decreased significance can be observed in θ when MN acts as driver, alone towards the system {DMN,ECN} or in conjunction with DMN toward ECN. In Fig.1 (a), we report the population distributions of global OIR $\Omega_{DMN,ECN,MN}$ in the three frequency bands. We observe overall positive values both at T0 ($\Omega(\theta) = 0.04 \pm 0.04$; $\Omega(\alpha) = 0.08 \pm 0.05$; $\Omega(\beta) = 0.17 \pm 0.17$) and T1 ($\Omega(\theta) = 0.03 \pm 0.06$; $\Omega(\alpha) = 0.07 \pm 0.06$; $\Omega(\beta) = 0.16 \pm 0.21$), indicating the prevalence of redundancy in the interactions among the three RSNs investigated. On average, decreasing values can be noticed at T1, especially at θ, in which we found a significant T1 – T0 difference ($p = 0.049$), and α frequencies. Although OIR is still positive, on average, this trend suggests a relative shift toward less redundant and more synergistic values in the overall balance described by the OIR metric after the rehabilitation. The average $\Omega_{DMN,ECN,MN}$ decrease at T1 is observed also in the causal decomposition of the spectral OIR, considering each of the three RSNs in turn as target process (Fig. 1 (b)). In particular, considering the statistically

 # % significant connections ($\alpha_s = 0.05$)

targets	drivers	DMN T0	DMN T1	ECN T0	ECN T1	MN T0	MN T1
θ	DMN			22	27	16	28
	ECN	60	63			23*	38
	MN	56	51	53	54		
α	DMN			21	29	18*	32
	ECN	56	57			19**	39
	MN	57	44	50	45		
β	DMN			55	56	59	61
	ECN	74	81			56	66
	MN	79	73	73	69		

100 %
0

Fig. 3 CFT surrogate analysis for pairwise directed functional connectivity measure. In each table, one for each frequency, percentages of csGC significant connections in the whole population are reported at both T0 and T1. Asterisks indicate a statistically T1 – T0 difference, *, p-value < 0.05, **, p-value < 0.01.

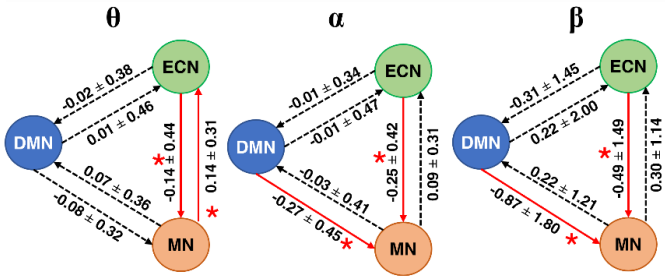

Fig. 4. T1 – T0 differences of inter-network csGC estimated for each directed pairwise connection (mean ± std). Red arrows indicate statistically different connection, *, p-value < 0.05, **, p-value < 0.01.

This work is licensed under a Creative Commons Attribution-NonCommercial-NoDerivatives 4.0 License. For more information, see https://creativecommons.org/licenses/by-nc-nd/4.0/

This article has been accepted for publication in IEEE Transactions on Neural Systems and Rehabilitation Engineering. This is the author's version which has not been fully edited and content may change prior to final publication. Citation information: DOI 10.1109/TNSRE.2023.3332114

significant T1 – T0 differences, the increasing synergy/decreasing redundancy ($\Omega^{T1-T0}_{DMN,ECN,MN} < 0$) in the overall balance behavior of the system appears to be mostly explained by the MN acting as driver in two main cases: by its-own towards the rest of the system in θ and α (p(θ) = 0.005 and p(α) = 0.009), and in combination with ECN as a driver towards DMN at all the considered frequency bands. Only in the α band, we found a mild (p(α) = 0.037) significant reduction of causality for ECN considered as a target of the vector process {DMN, MN}. Conversely, the ECN seems to play a role in the recovery of motor functions, especially of the upper limb. As shown in Fig. 2, we found a negative correlation between Ω^{T1-T0} and FMA^{T1-T0} when ECN acts as a driver towards the process {DMN, MN} in both θ and α frequencies, and when ECN is driver in pairs with DMN towards MN in θ. Hence, increase in synergy driven by ECN appears to correlate with upper limb motor recovery. In Fig. 3, the CFT surrogate data analysis shows that the most represented connections (dark green) are those from DMN towards both ECN and MN, and the ones from ECN to MN, both at T0 and T1. Besides, at T1 with respect to T0, we found a significant increase of connections from MN to ECN in θ and α (Δ#MN→ECN(θ) = 15 %, p(θ) = 0.015; Δ#MN→ECN(α) = 20 %, p(α) = 0.001). Always in α, a significant increase of the number of connections from MN to DMN was observed, Δ#MN→DMN(α) = 15 %, p(α) = 0.012. In Fig. 4, we report the average (± std) difference between csGC at T1 with respect to T0. Consistently with the surrogate binary analysis, at all frequencies we observe a reduction of weighted connectivity strength towards the MN target originating from DMN and ECN. Conversely, an increase of outflow from MN is observed towards ECN at all frequencies and towards DMN in β band. Specifically, the weight of direct connection DMN→MN significantly decreases in α (p = 0.013) and β (p = 0.049), whereas the connection ECN→MN significantly decreases in θ (p = 0.03) and α (p = 0.013) bands. The link MN→ECN significantly increases only in θ (p = 0.041). Finally, we also calculated the NFI to account for the net flow between inwards and outwards information transfer in each node (Fig. 5). At all frequencies, we observe a T1-T0 increase in the net flow directed from DMN to ECN and a T1-T0 decrease in the MN in-flow. The topology resulting from the NFI calculation highlights the presence of a direct connection DMN→MN, plus a DMN→ECN→MN chain of information flow, which also provide an indirect communication route from DMN to MN. Moreover, as reported in Fig. 6, we found that the variation $csGC^{T1-T0}_{ECN\rightarrow DMN}$ in the α band positively correlated with lower limb motor outcome FAC^{T1-T0} (r = 0.51, p = 0.032), whereas the increase of $csGC^{T1-T0}_{MN\rightarrow ECN}$ in θ positively correlated with FAC^{T1-T0} (r = 0.48, p = 0.045). Thus, improvements in ambulatory performance correlate with increased direct connectivity ECN → DMN in α and increased MN→ECN in θ.

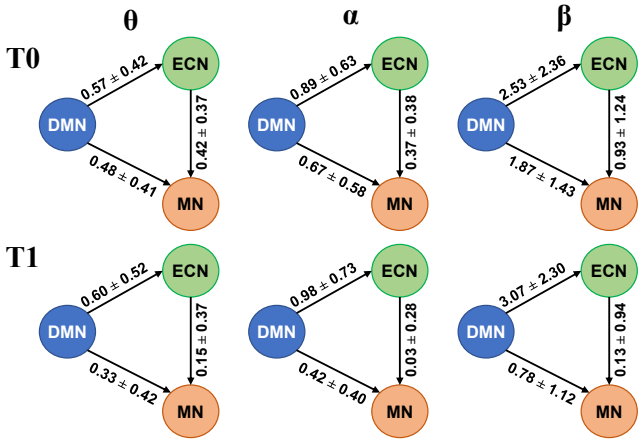

Fig. 5. Weighted net flow index (NFI) between large-scale networks based on conditional spectral granger causality estimation, T0 and T1 (rows) and for θ, α, and β frequencies (columns).

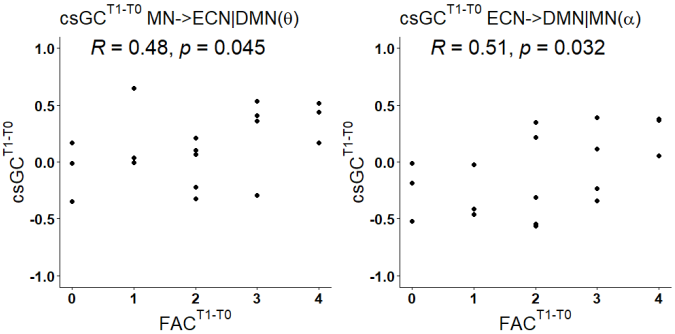

Fig. 6. Significant Spearman's correlations between csGC variations T1-T0 and FAC^{T1-T0}. R, correlation coefficient, p, p-value.

IV. Discussion

The main goal of this work was to investigate HOIs among three RSNs, i.e., DMN, ECN and MN, to identify their changes after rehabilitation of subacute stroke patients. All the previous studies only investigated pairwise interactions between these networks or the correlation of intra-network connectivity with functional impairment in different domains [50], while there is a lack in the characterization of their HOIs. Moreover, it is unclear whether the three interacting networks act synergistically or redundantly in stroke patients. For this reason, alongside the pairwise connectivity descriptors, we provided also a high-order characterization of these interactions using OIR, to investigate the causal processes underlying the redundant/synergic behavior among the three RSNs.

A. HOIs

In our analysis, we found a prevalence of redundancy (positive OIR values) in the interactions among the RSNs examined at all the frequency bands of interest, both before and after the rehabilitation. In addition, in our longitudinal evaluation of subacute stroke recovery, we observed a relative increase of shift toward less redundant and more synergistic values among DMN, ECN, and MN, which reached significance in θ frequency. Looking at the causal decomposition of the OIR, we found that this decrease in net redundancy appeared prevalently when MN acts alone as driver towards the other two networks, or when ECN and MN jointly drive DMN. More specifically, we found a significant increase of causal influence from T0 to T1, especially in α and θ frequencies

In the literature, the description of high-order brain networks characteristics is very limited. Up to date, very few works

This work is licensed under a Creative Commons Attribution-NonCommercial-NoDerivatives 4.0 License. For more information, see https://creativecommons.org/licenses/by-nc-nd/4.0/

This article has been accepted for publication in IEEE Transactions on Neural Systems and Rehabilitation Engineering. This is the author's version which has not been fully edited and content may change prior to final publication. Citation information: DOI 10.1109/TNSRE.2023.3332114

investigated the synergistic/redundant behavior within RSNs in healthy subjects, and, to our knowledge, no one has previously investigated a post-stroke population. Antonacci *et al.* [15], explored the functional interactions among different cortical areas during movement execution in normal subjects. In their work, dynamic EEG measures of high-order connectivity at the sensor level in the frequency domain highlighted the presence of redundancy among MN and frontal areas. This result agrees with our findings.

Luppi *et al.* [14] provided a first description of neuronal profiles for synergy and redundancy of different RSNs to analyze resting state functional MRI data from 100 healthy participants of the Human Connectome Project. They found that redundancy tends to prevail within RSNs, in particular in MN, visual and salience networks, while synergistic interactions are stronger between RSNs, especially between DMN and frontoparietal regions belonging to ECN. However, these results are not directly comparable with ours since different conceptual definitions of redundancy and synergy were used. Indeed, they considered a pairwise approach, in which target and driver variables are defined based on their present and past states, evolving jointly over time. Moreover, it should be noted that, even when the same conceptual framework is applied, different sensitivity in determining the balance between redundancy and synergy across positive and negative values can be expected depending on the method used to assess such balance. For instance, metrics based on entropy tends to emphasize synergy over redundancy with respect to metrics based on variance; this effect is related to the nonlinearity of the logarithmic function used by the metrics based on entropy, that has been verified in theoretical simulations [51] and experimental data [52], [53]. Therefore, care should be taken when making a comparison among different studies assessing high-order interactions in complex systems, and future comparative works are encouraged to assess redundant and synergistic contributions before and after rehabilitation, to confirm and complement the results of the present work.

B. Pairwise interactions

As for pairwise interactions, we observed a significant reduction in weighted directed connectivity from DMN and ECN towards MN after rehabilitation therapy in α and β rhythms. On the other hand, we found a significant increased connectivity of MN outwards link only for the connection MN→ECN in θ. We can speculate that MN, after rehabilitation, is less influenced by DMN and ECN activity and, conversely, provides more feedback to high-order control networks, since it recovers some specific functionalities. On the other hand, we found a significant increased connectivity of MN outwards link only for the connection MN→ECN in θ. The role of θ band in stroke recovery has been previously observed by [54], and it has been related to the coordination of sensory and motor brain activities during the execution of complex motor task that require spatial and motor learning [55]. Since we investigated not only the brain primary motor circuits, but also the interactions with high-order cognitive control networks, the θ role in complex motor coordination could have been particularly emphasized. Moreover, we point out that in our results a consistent increasing trend from T0 to T1 across all frequencies was found, albeit without reaching statistical significance in α and β. Increasing the sample size could provide more robust statistical significance besides θ.

A resting state fMRI study by Wang *et al.* [56], which investigated the role of large-scale network in the recovery of chronic stroke patients who followed a robot guided rehabilitation protocol, found that after rehabilitation in DMN and MN there was a significant increase in brain network temporal variability, a measure related to the strength of functional connectivity. Similarly, a fMRI study in chronic stroke patients by Wu *et al.* [21] found an increased functional connectivity between DMN and MN areas after motor rehabilitation, with an enhancement of specific connections that was positively associated with motor performance. These results appear to be in contrast with our findings. However, it should be considered that the two cited studies did not investigate directional causal relationship between networks, but only undirected functional connectivity. Thus, these results are not directly comparable to those we obtained by applying directed causal connectivity analysis (OIR and csGC). Besides, differently from the two cited studies [21], [56] which investigated chronic stroke patients, we considered patients in an early subacute stage. In the subacute stage, the affected brain tissue may be relatively more prone to benign neuroplastic reorganization, for instance due to perilesional edema reabsorption or synaptic formation [57], which may promote recovery of function in the MN, thus, as discussed above, disengaging it from vicarious support provided by ECN and DMN influences. Conversely, in the chronic stage, the motor system may be less liable to neurophysiological reactivation [58]. Thus, recovery in the chronic stage may be relatively more dependent on compensatory mechanisms, such that increased influences originating from ECN and DMN may act on the MN to at least partially drive functional restoration.

Our results on NFI, which account for the balance between inwards and outwards information flux for each node, suggest that DMN may act as a common driver for MN and ECN. Alongside a direct influence from DMN upon the recovering MN, ECN may play the role of mediator in the communication between DMN and MN. Again, the influence of the two high-order cognitive networks over the MN appears to reduce after the rehabilitation. We can speculate that these inter-network dynamics may reflect the exploitation of various strategies in stroke patients at T0, particularly combining proprioceptive and self-referential cues (DMN, [25]) with executive control mechanisms (ECN, [26]) in attempting to overcome the motor impairment. Rehabilitation may promote (partial) recovery of function in the MN, thus weakening these inter-network dynamics at T1 compared to T0.

C. Correlations with Clinical Outcomes

The literature on the correlation between connectivity measures and motor outcome in stroke is very heterogeneous and often contradictory, therefore further studies confirming the actual usefulness of these metrics in relation to post-stroke

This work is licensed under a Creative Commons Attribution-NonCommercial-NoDerivatives 4.0 License. For more information, see https://creativecommons.org/licenses/by-nc-nd/4.0/

This article has been accepted for publication in IEEE Transactions on Neural Systems and Rehabilitation Engineering. This is the author's version which has not been fully edited and content may change prior to final publication. Citation information: DOI 10.1109/TNSRE.2023.3332114

motor rehabilitation are needed [59]. Several factors contribute to the heterogeneity of the current results, including the diversity of rehabilitation protocols, e.g., conventional, motor imagery, with or without Brain Computer Interface (BCI) [60], the time post-stroke when the measurements are made, the different degree of functional recovery achieved by the subjects, and the clinical scales used for correlation studies that often focus only on the upper limbs [59], [61]. In addition, the diversity of neuroimaging techniques and connectivity analysis metrics, such as functional connectivity, effective connectivity and lately high-order interactions measures, contribute to the heterogeneity of the results and the selection of the most appropriate measure as recovery biomarker is still an open issue. One of the most consistent result in the literature is the link between motor recovery and reduction of interhemispheric connectivity between primary motor regions [62], [63], which also found to be influenced by the degree of motor recovery [64]. However, it has been observed that functional recovery post-stroke is associated also with the interaction of different RSNs with the MN, since also cognitive networks are involved in neuroplasticity processes [65]. However, large-scale networks interaction effects have not been reported widely across the literature and thus require additional studies [59]. The present work fits into this context of investigation of RSNs interactions, trying to add knowledge to the existing literature. In our study we found some interesting correlations between connectivity metrics and clinical motor recovery scales. In particular, considering the high-order approach, the increased interactions and synergy when ECN acts as a driver towards the other networks are significantly correlated to the recovery of upper limb motor function, measured as FMA score. Even though a statistically significant increase in synergy was observed in HOIs involving MN as a driver and DMN as a target, no correlation with motor outcome was found for these interactions. Furthermore, even in the case of pairwise analysis, an increased causal connectivity between ECN and DMN, as well as between MN and ECN, was correlated with motor performance, in particular of the lower limb (FAC scale). We speculate that the observed difference in changes of RSNs interactions for upper and lower limb recovery may be due in the first instance to the EEG different sensitivity to the larger upper limb cortical representation and the proximity to the scalp electrodes as compared to the lower limb [66]. Moreover, from a neurophysiological perspective, we hypothesize that the walking functionality measured by the FAC requires more integration and information exchange between MN and the other cognitive networks (DMN and ECN), as compared to a simple arm movement assessed with the FMA. Therefore, the pairwise connectivity ECN→ DMN and MN → ECN may be more relevant for lower limb measures, as they reflect the coordination of these cognitive processes during walking, whereas for the HOIs the joint involvement of two RSNs may blur this effect. All these results may suggest the involvement of ECN in motor functionality recovery, as previously hypothesized [22], [67]. However, this hypothesis should be further investigated and supported by studies in larger populations. It is noteworthy that we found the statistically significant correlations of RSNs interaction and motor recovery scales only in lower frequencies, θ and α bands. In agreement with our findings, previous studies have described the role of θ and α in the interaction between MN with other networks involved in other cognitive processes [54], [59], [68].

However, previous studies have also reported a correlation between β functional connectivity metrics and upper limb motor recovery in different settings [69]. In particular, the correlation in β has been observed in studies on motor imagery protocol rehabilitation using BCI [60], [70]. Pichiorri and colleagues [60] reported a comparison of effective connectivity estimated in a group of patients who underwent a BCI guided therapy with another group who received the same rehabilitation protocol without BCI. In agreement with [70], they found a correlation with FMA scale in β and γ only in the BCI group, suggesting a more effective impact of BCI in the functional recovery of stroke patients. Conversely, they did not find this correlation for the non-BCI group, in a population similar to ours.

D. Limits of the work and future developments

In our study we found a high variability in EEG derived metrics among subjects. This variability could be due to individual differences in brain activation, also caused by different locations of focal cortical and sub-cortical brain damages. The small sample size may represent a further limitation of this study, an increase of patients to be involved may improve the reliability and robustness of the population's OIR estimates and their correlations with clinical outcomes. As for the correlation analysis, the most significant results have been observed concerning upper limb recovery scale. However, the results should be confirmed on a larger and more homogeneous population to evince the ECN involvement.

Besides the three RSNs here investigated, other RSNs changes have been found to be involved in stroke recovery, such as the dorsal and ventral attention or language networks [50] as well as the auditory and the visual networks [16], [22]. Being based on linear parametric modeling, OIR requires a standard technique for the identification of the VAR model, such as the ordinary least square or the Levison's algorithm for the solution of the Yule-walker equations. However, to avoid the increasing of bias and variance of estimation, which may result in ill-posed regression problems, the ratio between the amount of data samples available and the number of regression coefficients to be estimated should be at least equal to 10 to guarantee the accuracy of the estimation procedure [71], [72]. For this reason, we focused our analysis on three of the main RSNs known to be affected by stroke, without excessively increasing the number of time series to be fitted. In our case, we had 1280 samples available for each time series, and we could not fit more than the 16 selected ROIs, otherwise the goodness of the estimated autoregressive parameters would not be guaranteed. The 16 ROIs have been selected on the bases of previous literature in the field [39]–[41], using the centroids' coordinates provided in the MNI space according to the template we employed for the source reconstruction and obtaining areas of comparable volume size. Besides the efforts

This work is licensed under a Creative Commons Attribution-NonCommercial-NoDerivatives 4.0 License. For more information, see https://creativecommons.org/licenses/by-nc-nd/4.0/

This article has been accepted for publication in IEEE Transactions on Neural Systems and Rehabilitation Engineering. This is the author's version which has not been fully edited and content may change prior to final publication. Citation information: DOI 10.1109/TNSRE.2023.3332114

to be consistent with previous works, it should be considered that changes in the selection of ROIs and definition of conduction volume in the source reconstruction may induce changes in the results obtained. However, considering the limited spatial resolution of EEG (about 1 – 2 cm), a small variation ROI size around the same centroid's coordinates should have a relatively small effect.

As for the causal interpretation of the individual network contribution to the inter-network increase in synergy, we should point out that the driver role of MN and ECN cannot be stated with total confidence. In fact, in our data, the instantaneous causality term which appears in (9) is not null; thus, we cannot affirm that the directionality terms totally explain the redundancy/synergy balance. Indeed, the strict causality hypothesis [45] should be fulfilled to account exclusively for the directionality terms. However, the instantaneous synchronization is intrinsic in EEG techniques, and even though mitigated by source activity reconstruction, we could not completely overcome this issue. In future, this aspect should be further investigated. Besides, the OIR approach proves to be powerful for the investigation of HOIs in connectivity adding spectral and directional description. This method could be interestingly applied for the simultaneous investigation of a larger number of networks, but still, at the cost of lower-spatial resolution to obtain a lower number of cortical areas for each large-scale network. Finally, considering the recent literature in which HOIs were observed in healthy subjects [73], [74], a study on an aged-matched control population with the same metric here employed may be interesting to support our interpretations, eliminating those confounding factors that can arise considering only pathological individuals.

V. Conclusion

The use of high-order interaction metrics, like OIR, in addition to pairwise approach, in the study of inter network connectivity in stroke patients could be a powerful tool for better understanding complex multiple relationships among RSNs, giving a particular focus on their redundant/synergistic behavior. Adopting this perspective, in our study we found a predominance of redundant interactions among the RSNs both before and after the rehabilitation in subacute stroke. After rehabilitation, we observed an increased shift toward less redundant and more synergistic behavior, mainly related to the joint effect of MN and ECN on DMN. As to the pairwise connectivity analysis, we observed a reduction of both DMN and ECN influence over MN. Finally, the correlation analysis with clinical outcomes, suggests that ECN may be an interesting player in motor functionality improvement, even though further investigations are needed to better comprehend its role.

References

[1] M. Rubinov and O. Sporns, "Complex network measures of brain connectivity: Uses and interpretations," *Neuroimage*, vol. 52, no. 3, pp. 1059–1069, Sep. 2010, doi: 10.1016/J.NEUROIMAGE.2009.10.003.

[2] M. Günther, J. W. Kantelhardt, and R. P. Bartsch, "The Reconstruction of Causal Networks in Physiology," *Front. Netw. Physiol.*, vol. 2, p. 25, May 2022, doi: 10.3389/FNETP.2022.893743.

[3] L. Faes, D. Marinazzo, G. Nollo, and A. Porta, "An Information-Theoretic Framework to Map the Spatiotemporal Dynamics of the Scalp Electroencephalogram," *IEEE Trans. Biomed. Eng.*, vol. 63, no. 12, pp. 2488–2496, Dec. 2016, doi: 10.1109/TBME.2016.2569823.

[4] R. Herzog *et al.*, "Genuine high-order interactions in brain networks and neurodegeneration," *Neurobiol. Dis.*, vol. 175, no. August, 2022, doi: 10.1016/j.nbd.2022.105918.

[5] S. Yu, H. Yang, H. Nakahara, G. S. Santos, D. Nikolić, and D. Plenz, "Higher-Order interactions characterized in cortical activity," *J. Neurosci.*, vol. 31, no. 48, pp. 17514–17526, 2011, doi: 10.1523/JNEUROSCI.3127-11.2011.

[6] E. Ganmor, R. Segev, and E. Schneidman, "Sparse low-order interaction network underlies a highly correlated and learnable neural population code," *Proc. Natl. Acad. Sci. U. S. A.*, vol. 108, no. 23, pp. 9679–9684, 2011, doi: 10.1073/pnas.1019641108.

[7] F. Battiston *et al.*, "Networks beyond pairwise interactions: Structure and dynamics," *Phys. Rep.*, vol. 874, no. June, pp. 1–92, 2020, doi: 10.1016/j.physrep.2020.05.004.

[8] W. J. McGill, "Multivariate information transmission," *IRE Prof. Gr. Inf. Theory*, vol. 4, no. 4, pp. 93–111, 1954, doi: 10.1109/TIT.1954.1057469.

[9] P. L. Williams and R. D. Beer, "Nonnegative Decomposition of Multivariate Information," Apr. 2010, Accessed: May 04, 2023. [Online]. Available: https://arxiv.org/abs/1004.2515v1.

[10] F. E. Rosas, P. A. M. Mediano, M. Gastpar, and H. J. Jensen, "Quantifying high-order interdependencies via multivariate extensions of the mutual information," *Phys. Rev. E*, vol. 100, no. 3, p. 032305, Sep. 2019, doi: 10.1103/PHYSREVE.100.032305/FIGURES/9/MEDIUM.

[11] L. Faes *et al.*, "A New Framework for the Time-and Frequency-Domain Assessment of High-Order Interactions in Networks of Random Processes," *IEEE Trans. Signal Process.*, vol. 70, pp. 5766–5777, 2022, doi: 10.1109/TSP.2022.3221892.

[12] M. Andjelković, B. Tadić, and R. Melnik, "The topology of higher-order complexes associated with brain hubs in human connectomes," *Sci. Rep.*, vol. 10, no. 1, pp. 1–10, 2020, doi: 10.1038/s41598-020-74392-3.

[13] M. Gatica *et al.*, "High-Order Interdependencies in the Aging Brain," *Brain Connect.*, vol. 11, no. 9, pp. 734–744, 2021, doi: 10.1089/brain.2020.0982.

[14] A. I. Luppi *et al.*, "A synergistic core for human brain evolution and cognition," *Nat. Neurosci.*, vol. 25, no. 6, pp. 771–782, 2022, doi: 10.1038/s41593-022-01070-0.

[15] Y. Antonacci *et al.*, "Measuring high-order interactions in rhythmic processes through multivariate spectral information decomposition," *IEEE Access*, vol. 9, pp. 149486–149505, 2021, doi: 10.1109/ACCESS.2021.3124601.

[16] J. S. Siegel *et al.*, "Disruptions of network connectivity predict impairment in multiple behavioral domains after stroke," *Proc. Natl. Acad. Sci. U. S. A.*, vol. 113, no. 30, pp. E4367–E4376, 2016, doi: 10.1073/pnas.1521083113.

[17] C. Grefkes and G. R. Fink, "Reorganization of cerebral networks after stroke: new insights from neuroimaging with connectivity approaches," *BRAIN A J. Neurol.*, vol. 134, pp. 1264–1276, 2011, doi: 10.1093/brain/awr033.

[18] B. Hordacre, M. R. Goldsworthy, E. Welsby, L. Graetz, S. Ballinger, and S. Hillier, "Resting State Functional Connectivity Is Associated With Motor Pathway Integrity and Upper-Limb Behavior in Chronic Stroke," *Neurorehabil. Neural Repair*, vol. 34, no. 6, pp. 547–557, Jun. 2020, doi: 10.1177/1545968320921824.

[19] C. Stinear, "Prediction of recovery of motor function after stroke," *Lancet. Neurol.*, vol. 9, no. 12, pp. 1228–1232, Dec. 2010, doi: 10.1016/S1474-4422(10)70247-7.

[20] C. Wang *et al.*, "Altered functional organization within and between resting-state networks in chronic subcortical infarction," *J. Cereb. Blood Flow Metab.*, vol. 34, no. 4, pp. 597–605, 2014, doi: 10.1038/jcbfm.2013.238.

[21] C. W. Wu *et al.*, "Synchrony Between Default-Mode and Sensorimotor Networks Facilitates Motor Function in Stroke Rehabilitation: A Pilot fMRI Study," *Front. Neurosci.*, vol. 14, no. June, pp. 1–11, 2020, doi: 10.3389/fnins.2020.00548.

This work is licensed under a Creative Commons Attribution-NonCommercial-NoDerivatives 4.0 License. For more information, see https://creativecommons.org/licenses/by-nc-nd/4.0/

This article has been accepted for publication in IEEE Transactions on Neural Systems and Rehabilitation Engineering. This is the author's version which has not been fully edited and content may change prior to final publication. Citation information: DOI 10.1109/TNSRE.2023.3332114

[22] Z. Zhao *et al.*, "Altered intra- and inter-network functional coupling of resting-state networks associated with motor dysfunction in stroke," *Hum. Brain Mapp.*, vol. 39, no. 8, pp. 3388–3397, 2018, doi: 10.1002/hbm.24183.

[23] Z. Zhao *et al.*, "Altered effective connectivity of the primary motor cortex in stroke: A resting-state fMRI study with granger causality analysis," *PLoS One*, vol. 11, no. 11, Nov. 2016, doi: 10.1371/journal.pone.0166210.

[24] G. Doucet *et al.*, "Brain activity at rest: A multiscale hierarchical functional organization," *J. Neurophysiol.*, vol. 105, no. 6, pp. 2753–2763, 2011, doi: 10.1152/JN.00895.2010/SUPPL_FILE/TABLES6.PDF.

[25] M. E. Raichle, A. M. MacLeod, A. Z. Snyder, W. J. Powers, D. A. Gusnard, and G. L. Shulman, "A default mode of brain function," *Proc. Natl. Acad. Sci. U. S. A.*, vol. 98, no. 2, pp. 676–682, Jan. 2001, doi: 10.1073/PNAS.98.2.676/ASSET/0D756665-76C2-42A2-ACA7-01DE9C6DEDA4/ASSETS/GRAPHIC/PQ0115125005.JPEG.

[26] M. Corbetta and G. L. Shulman, "Control of goal-directed and stimulus-driven attention in the brain," *Nat. Rev. Neurosci. 2002 33*, vol. 3, no. 3, pp. 201–215, 2002, doi: 10.1038/nrn755.

[27] W. W. Seeley *et al.*, "Dissociable intrinsic connectivity networks for salience processing and executive control," *J. Neurosci.*, vol. 27, no. 9, pp. 2349–2356, 2007, doi: 10.1523/JNEUROSCI.5587-06.2007.

[28] H. Liu, T. Tian, W. Qin, K. Li, and C. Yu, "Contrasting evolutionary patterns of functional connectivity in sensorimotor and cognitive regions after stroke," *Front. Behav. Neurosci.*, vol. 10, no. APRIL, p. 72, Apr. 2016, doi: 10.3389/FNBEH.2016.00072/BIBTEX.

[29] Q. Wu *et al.*, "Brain Functional Networks Study of Subacute Stroke Patients With Upper Limb Dysfunction After Comprehensive Rehabilitation Including BCI Training," *Front. Neurol.*, vol. 10, Jan. 2020, doi: 10.3389/fneur.2019.01419.

[30] E. Olafson *et al.*, "Frontoparietal network activation is associated with motor recovery in ischemic stroke patients," *Commun. Biol. 2022 51*, vol. 5, no. 1, pp. 1–11, Sep. 2022, doi: 10.1038/s42003-022-03950-4.

[31] I. Pirovano *et al.*, "Resting State EEG Directed Functional Connectivity Unveils Changes in Motor Network Organization in Subacute Stroke Patients After Rehabilitation," *Front. Physiol.*, vol. 13, no. April, pp. 1–14, 2022, doi: 10.3389/fphys.2022.862207.

[32] A. R. Fugl-Meyer, L. Jääskö, I. Leyman, S. Olsson, and S. Steglind, "The post-stroke hemiplegic patient. 1. a method for evaluation of physical performance.," *Scand. J. Rehabil. Med.*, vol. 7, no. 1, pp. 13–31, 1975.

[33] M. Holden, K. Gill, M. Magliozzi, J. Nathan, and L. Piehl-Baker, "Clinical gait assessment in the neurologically impaired. Reliability and meaningfulness," *Phys. Ther.*, vol. 64, no. 1, pp. 35–40, 1984, doi: 10.1093/PTJ/64.1.35.

[34] A. Delorme and S. Makeig, "EEGLAB: an open source toolbox for analysis of single-trial EEG dynamics including independent component analysis," *J. Neurosci. Methods*, vol. 134, pp. 9–21, 2004.

[35] T. R. Mullen *et al.*, "Real-time neuroimaging and cognitive monitoring using wearable dry EEG," *IEEE Trans. Biomed. Eng.*, vol. 62, no. 11, pp. 2553–2567, 2015, doi: 10.1109/TBME.2015.2481482.

[36] S. Makeig and A. J. Bell, "Independent Component Analysis of Electroencephalographic Data," in *Proceedings of the 8th International Conference on Neural Information Processing Systems*, 1996, p. 145.151.

[37] L. Pion-Tonachini, K. Kreutz-Delgado, and S. Makeig, "ICLabel: An automated electroencephalographic independent component classifier, dataset, and website," *Data Br.*, vol. 25, p. 104101, 2019.

[38] R. D. Pascual-Marqui, "Discrete, 3D distributed, linear imaging methods of electric neuronal activity. Part 1: exact, zero error localization," Oct. 2007, [Online]. Available: http://arxiv.org/abs/0710.3341.

[39] M. E. Raichle, "The restless brain," *BRAIN Connect.*, vol. 1, no. 1, 2011, doi: 10.1089/brain.2011.0019.

[40] C. S. Inman, G. A. James, S. Hamann, J. K. Rajendra, G. Pagnoni, and A. J. Butler, "Altered resting-state effective connectivity of fronto-parietal motor control systems on the primary motor network following stroke," *Neuroimage*, vol. 59, no. 1, pp. 227–237, Jan. 2012, doi: 10.1016/j.neuroimage.2011.07.083.

[41] J. Samogin *et al.*, "Frequency-dependent functional connectivity in resting state networks," *Hum. Brain Mapp.*, vol. 41, no. 18, pp. 5187–5198, 2020, doi: 10.1002/hbm.25184.

[42] L. Faes, S. Erla, and G. Nollo, "Measuring Connectivity in Linear Multivariate Processes: Definitions, Interpretation, and Practical Analysis," *Comput. Math. Methods Med.*, vol. 2012, 2012, doi: 10.1155/2012/140513.

[43] C. W. J. Granger, "Investigating Causal Relations by Econometric Models and Cross-spectral Methods," *Econometrica*, vol. 37, no. 3, pp. 424–438, 1969.

[44] J. Geweke, "Measurement of linear dependence and feedback between multiple time series," *J. Am. Stat. Assoc.*, vol. 77, no. 378, pp. 304–313, 1982, doi: 10.1080/01621459.1982.10477803.

[45] D. Chicharro, "On the spectral formulation of Granger causality," *Biol. Cybern.*, vol. 105, no. 5–6, pp. 331–347, 2011, doi: 10.1007/s00422-011-0469-z.

[46] J. F. Geweke, "Measures of Conditional Linear Dependence and Feedback Between Time Series Author (s): John F . Geweke Source : Journal of the American Statistical Association , Vol . 79 , No . 388 (Dec ., 1984), pp . 907-," *J. Am. Stat. Assoc.*, vol. 79, no. 388, pp. 907–915, 1984, [Online]. Available: https://www.tandfonline.com/doi/abs/10.1080/01621459.1984.10477110.

[47] W. Klimesch, "EEG alpha and theta oscillations reflect cognitive and memory performance: A review and analysis," *Brain Res. Rev.*, vol. 29, no. 2–3, pp. 169–195, 1999, doi: 10.1016/S0165-0173(98)00056-3.

[48] J. Theiler, S. Eubank, A. Longtin, B. Galdrikian, and J. Doyne Farmer, "Testing for nonlinearity in time series: the method of surrogate data," *Phys. D*, vol. 58, pp. 77–94, 1992.

[49] L. Faes, A. Porta, and G. Nollo, "Testing frequency-domain causality in multivariate time series," *IEEE Trans. Biomed. Eng.*, vol. 57, no. 8, pp. 1897–1906, 2010, doi: 10.1109/TBME.2010.2042715.

[50] Z. Romeo, D. Mantini, E. Durgoni, L. Passarini, F. Meneghello, and M. Zorzi, "Electrophysiological signatures of resting state networks predict cognitive deficits in stroke," *Cortex*, vol. 138, pp. 59–71, May 2021, doi: 10.1016/j.cortex.2021.01.019.

[51] A. B. Barrett, "Exploration of synergistic and redundant information sharing in static and dynamical Gaussian systems," *Phys. Rev. E - Stat. Nonlinear, Soft Matter Phys.*, vol. 91, no. 5, 2015, doi: 10.1103/PhysRevE.91.052802.

[52] A. Porta *et al.*, "Quantifying Net Synergy/Redundancy of Spontaneous Variability Regulation via Predictability and Transfer Entropy Decomposition Frameworks," *IEEE Trans. Biomed. Eng.*, vol. 64, no. 11, pp. 2628–2638, 2017, doi: 10.1109/TBME.2017.2654509.

[53] A. Porta *et al.*, "Categorizing the Role of Respiration in Cardiovascular and Cerebrovascular Variability Interactions," *IEEE Trans. Biomed. Eng.*, vol. 69, no. 6, pp. 2065–2076, 2022, doi: 10.1109/TBME.2021.3135313.

[54] N. Rustamov, J. Humphries, A. Carter, and E. C. Leuthardt, "Theta-gamma coupling as a cortical biomarker of brain-computer interface-mediated motor recovery in chronic stroke," *Brain Commun.*, vol. 4, no. 3, 2022, doi: 10.1093/braincomms/fcac136.

[55] J. B. Caplan, J. R. Madsen, A. Schulze-Bonhage, R. Aschenbrenner-Scheibe, E. L. Newman, and M. J. Kahana, "Human θ oscillations related to sensorimotor integration and spatial learning," *J. Neurosci.*, vol. 23, no. 11, pp. 4726–4736, 2003, doi: 10.1523/jneurosci.23-11-04726.2003.

[56] X. Wang, W. W. Wong, R. Sun, W. C. W. Chu, and K. Y. Tong, "Differentiated effects of robot hand training with and without neural guidance on neuroplasticity patterns in chronic stroke," *Front. Neurol.*, vol. 9, no. OCT, pp. 1–13, 2018, doi: 10.3389/fneur.2018.00810.

[57] C. Grefkes, C. Grefkes, G. R. Fink, and G. R. Fink, "Recovery from stroke: current concepts and future perspectives," *Neurol. Res. Pract.*, vol. 2, no. 1, Jun. 2020, doi: 10.1186/S42466-020-00060-6.

[58] R. A. Mooney, J. Cirillo, C. M. Stinear, and W. D. Byblow, "Neurophysiology of motor skill learning in chronic stroke," *Clin. Neurophysiol.*, vol. 131, no. 4, pp. 791–798, Apr. 2020, doi: 10.1016/J.CLINPH.2019.12.410.

[59] J. M. Cassidy, J. I. Mark, and S. C. Cramer, "Functional connectivity drives stroke recovery: shifting the paradigm from correlation to causation," *Brain*, vol. 145, no. 4, pp. 1211–1228,

This work is licensed under a Creative Commons Attribution-NonCommercial-NoDerivatives 4.0 License. For more information, see https://creativecommons.org/licenses/by-nc-nd/4.0/

This article has been accepted for publication in IEEE Transactions on Neural Systems and Rehabilitation Engineering. This is the author's version which has not been fully edited and content may change prior to final publication. Citation information: DOI 10.1109/TNSRE.2023.3332114

2022, doi: 10.1093/brain/awab469.

[60] F. Pichiorri *et al.*, "Brain-computer interface boosts motor imagery practice during stroke recovery," *Ann. Neurol.*, vol. 77, no. 5, pp. 851–865, May 2015, doi: 10.1002/ana.24390.

[61] G. Milani, A. Antonioni, A. Baroni, P. Malerba, and S. Straudi, "Relation Between EEG Measures and Upper Limb Motor Recovery in Stroke Patients: A Scoping Review," *Brain Topogr.*, vol. 35, no. 5–6, pp. 651–666, 2022, doi: 10.1007/s10548-022-00915-y.

[62] L. Wang *et al.*, "Dynamic functional reorganization of the motor execution network after stroke," *Brain*, vol. 133, no. 4, pp. 1224–1238, Apr. 2010, doi: 10.1093/brain/awq043.

[63] L. Cheng *et al.*, "Reorganization of Motor Execution Networks During Sub-Acute Phase After Stroke," *IEEE Trans. Neural Syst. Rehabil. Eng.*, vol. 23, no. 4, pp. 713–723, 2015, doi: 10.1109/TNSRE.2015.2401978.

[64] J. M. Cassidy *et al.*, "Low-Frequency Oscillations Are a Biomarker of Injury and Recovery after Stroke," *Stroke*, pp. 1442–1450, 2020, doi: 10.1161/STROKEAHA.120.028932.

[65] J. S. Siegel *et al.*, "Disruptions of network connectivity predict impairment in multiple behavioral domains after stroke," *Proc. Natl. Acad. Sci. U. S. A.*, vol. 113, no. 30, pp. E4367–E4376, Jul. 2016, doi: 10.1073/pnas.1521083113.

[66] N. Katagiri *et al.*, "Interindividual Variability of Lower-Limb Motor Cortical Plasticity Induced by Theta Burst Stimulation," *Front. Neurosci.*, vol. 14, no. November, pp. 1–10, 2020, doi: 10.3389/fnins.2020.563293.

[67] W. Geng *et al.*, "Reduced functional network connectivity is associated with upper limb dysfunction in acute ischemic brainstem stroke," *Brain Imaging Behav.*, vol. 16, no. 2, pp. 802–810, 2022, doi: 10.1007/s11682-021-00554-0.

[68] K. P. Westlake and S. S. Nagarajan, "Functional connectivity in relation to motor performance and recovery after stroke," *Frontiers in Systems Neuroscience*, no. MARCH 2011. Mar. 16, 2011, doi: 10.3389/fnsys.2011.00008.

[69] A. G. Guggisberg, P. J. Koch, F. C. Hummel, and C. Buetefisch, "Brain networks and their relevance for stroke rehabilitation," *Clin Neurophysiol*, vol. 130, no. 7, pp. 1098–1124, 2019, doi: 10.1016/j.clinph.2019.04.004.Brain.

[70] D. Rathee, A. Chowdhury, Y. K. Meena, A. Dutta, S. McDonough, and G. Prasad, "Brain-Machine Interface-Driven Post-Stroke Upper-Limb Functional Recovery Correlates with Beta-Band Mediated Cortical Networks," *IEEE Trans. Neural Syst. Rehabil. Eng.*, vol. 27, no. 5, pp. 1020–1031, 2019, doi: 10.1109/TNSRE.2019.2908125.

[71] Y. Antonacci, L. Astolfi, G. Nollo, and L. Faes, "Information Transfer in Linear Multivariate Processes Assessed through Penalized Regression Techniques: Validation and Application to Physiological Networks," *Entropy 2020, Vol. 22, Page 732*, vol. 22, no. 7, p. 732, Jul. 2020, doi: 10.3390/E22070732.

[72] A. Schlögl, "A comparison of multivariate autoregressive estimators," *Signal Processing*, vol. 86, no. 9, pp. 2426–2429, Sep. 2006, doi: 10.1016/J.SIGPRO.2005.11.007.

[73] A. I. Luppi *et al.*, "A synergistic workspace for human consciousness revealed by integrated information decomposition," *bioRxiv*, p. 2020.11.25.398081, 2020, [Online]. Available: https://doi.org/10.1101/2020.11.25.398081.

[74] T. F. Varley, M. Pope, J. Faskowitz, and O. Sporns, "Multivariate information theory uncovers synergistic subsystems of the human cerebral cortex," *Commun. Biol. 2023 61*, vol. 6, no. 1, pp. 1–12, Apr. 2023, doi: 10.1038/s42003-023-04843-w.

This work is licensed under a Creative Commons Attribution-NonCommercial-NoDerivatives 4.0 License. For more information, see https://creativecommons.org/licenses/by-nc-nd/4.0/